ATP and Magnesium Promote Cotton Short-Form Ribulose-1,5-bisphosphate Carboxylase/Oxygenase (Rubisco) Activase Hexamer Formation at Low Micromolar Concentrations

ARTICLE *in* BIOCHEMISTRY · OCTOBER 2014

Impact Factor: 3.02 · DOI: 10.1021/bi500968h · Source: PubMed

8 AUTHORS, INCLUDING:

Manas Chakraborty
University of Pennsylvania
7 PUBLICATIONS **23** CITATIONS
SEE PROFILE

Suratna Hazra
Arizona State University
3 PUBLICATIONS **12** CITATIONS
SEE PROFILE

Marcia Levitus
Arizona State University
54 PUBLICATIONS **1,464** CITATIONS
SEE PROFILE

BIOCHEMISTRY
including biophysical chemistry & molecular biology

Article

pubs.acs.org/biochemistry

ATP and Magnesium Promote Cotton Short-Form Ribulose-1,5-bisphosphate Carboxylase/Oxygenase (Rubisco) Activase Hexamer Formation at Low Micromolar Concentrations

Agnieszka M. Kuriata,[†,§] Manas Chakraborty,[†,‡,§] J. Nathan Henderson,[†] Suratna Hazra,[†] Andrew J. Serban,[†,‡] Tuong V. T. Pham,[†] Marcia Levitus,[†,‡] and Rebekka M. Wachter*[,†]

[†]Department of Chemistry and Biochemistry and Center for Bioenergy and Photosynthesis, Arizona State University, Tempe, Arizona 85287, United States

[‡]Biodesign Institute, Arizona State University, Tempe, Arizona 85287, United States

Supporting Information

ABSTRACT: We report a fluorescence correlation spectroscopy (FCS) study of the assembly pathway of the AAA+ protein ribulose-1,5-bisphosphate carboxylase/oxygenase (Rubisco) activase (Rca), a ring-forming ATPase responsible for activation of inhibited Rubisco complexes for biological carbon fixation. A thermodynamic characterization of simultaneously populated oligomeric states appears critical in understanding Rca structure and function. Using cotton β-Rca, we demonstrate that apparent diffusion coefficients vary as a function of concentration, nucleotide, and cation. Using manual fitting procedures, we provide estimates for the equilibrium constants for the stepwise assembly and find that in the presence of ATPγS, the K_d for hexamerization is 10-fold lower than with ADP (~0.1 vs ~1 μM). Hexamer fractions peak at 30 μM and dominate at 8−70 μM Rca, where they comprise 60−80% of subunits with ATPγS, compared with just 30−40% with ADP. Dimer fractions peak at 1−4 μM Rca, where they comprise 15−18% with ATPγS and 26−28% with ADP. At 30 μM Rca, large aggregates begin to form that comprise ~10% of total protein with ATPγS and ~25% with ADP. FCS data collected on the catalytically impaired WalkerB-D173N variant in the presence of ATP provided strong support for these results. Titration with free magnesium ions lead to the disaggregation of larger complexes in favor of hexameric forms, suggesting that a second magnesium binding site with a K_d value of 1−3 mM mediates critical subunit contacts. We propose that closed-ring toroidal hexameric forms are stabilized by binding of Mg·ATP plus Mg^{2+}, whereas Mg·ADP promotes continuous assembly to supramolecular aggregates such as spirals.

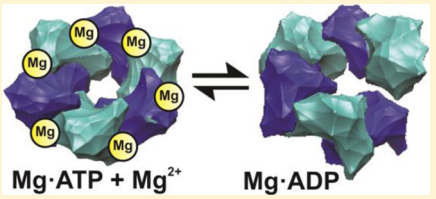

Rubisco [ribulose-1,5-bisphosphate (RuBP) carboxylase/oxygenase] is a central enzyme in photosynthesis, because it catalyzes the rate-limiting step in assimilation of inorganic CO_2 into organic building blocks responsible for all the world's biomass.[1] Implications for agronomic practices, biofuel production, and global carbon cycling ensure persistent interest in engineering or selecting for Rubisco enzymes with improved catalytic efficiency, with the ultimate goal of increasing crop yields.[2] A number of side reactions undermine Rubisco's carboxylation activity, especially the competing oxygenation of RuBP (ribulose 1,5-bisphosphate) that feeds the unproductive photorespiration pathway. When Rubisco first appeared on the early biotic earth, atmospheric CO_2 levels were many times higher and O_2 much lower than today, so O_2 competition with CO_2 for incorporation into RuBP was not significant.[3] As eons of oxygenic photosynthesis gradually raised O_2 levels at the expense of CO_2, evolution pushed Rubisco to bind RuBP more tightly, and opened avenues for regulation via nonproductive substrate binding and competitive inhibition by phosphorylated metabolites. Hence, a catalytic chaperone, known as Rubisco activase (Rca), came into play to restore activity to inactivated Rubisco complexes by releasing inhibitors through an as yet undetermined mechanism.[4] Within the chloroplast, the light-dependent stromal energy charge has been proposed to regulate Rca activity via the ATP/ADP ratio.[5] In species containing the redox-sensitive Rca α-isoform, additional regulation is afforded by the stromal redox potential.

Rca belongs to the AAA+ (ATPase associated with diverse cellular activities) superfamily of ATPases and is part of the extended group.[6] Despite diversity in sequence and function, a common theme with AAA+ proteins is the use of energy derived from ATP hydrolysis to perform chemomechanical work on substrate macromolecules. AAA+ proteins contain a structurally conserved ATP-binding cassette of approximately 200−250 residues consisting of a N-domain harboring the Walker A ($GX_4GK[T/S]$, where X can be any amino acid) and Walker B (Φ_4DE, where the Φ is hydrophobic residues) motifs, attached to a less conserved C-domain typically involved in substrate recognition. A cleft between the two domains provides a pocket for ATP binding, which frequently directs the formation of active multisubunit arrays.[7,8] The stoichiometries of AAA+ subunit assemblies are directly relevant to their

Received: August 4, 2014
Revised: October 29, 2014

   dx.doi.org/10.1021/bi500968h | *Biochemistry* XXXX, XXX, XXX−XXX

biological activity. Oligomerization brings neighboring protomers together, forming a bipartite ATP binding site with a conserved arginine (arginine finger) from one protomer interacting directly with the γ-phosphate of ATP bound to the adjacent protomer.[8] Presumably, this arrangement allows catalytic cycles involving ATP binding, hydrolysis, and ADP release to facilitate conformational changes that in turn mediate substrate remodeling or translocation events. Some AAA+ proteins require macromolecular binding partners to act as scaffolds for proper assembly,[9] and often there is a requirement for nucleotide binding.[10−13] Numerous reports suggest that assemblies with subunits in hexameric arrangements are most common,[13−17] though there are some exceptions.[18−20]

The highly polydisperse nature of protein preparations of Rca has long hampered mechanistic studies. Size exclusion chromatographs exhibit broad, asymmetric bands, suggesting concentration-dependent size distributions that range from monomers to extremely large aggregates of nearly 50 subunits.[21−24] However, recent work has demonstrated that gel filtration does not reflect equilibrium conditions, in line with rapid Rca subunit exchange.[24] Regardless, nucleotide-dependent Rca oligomerization appears to be essential for proper biological function,[21,23,25,26] and recent dynamic light scattering (DLS) experiments have confirmed that ATP, ADP, and Mg^{2+} increase self-association of cotton β-Rca.[24] Polydispersity was also observed by NanoESI mass spectrometry of wild-type tobacco Rca (Nt-β-Rca) in the presence of ADP, where sizes ranged up to hexameric forms.[27] However, the stable formation of a hexamer could only be demonstrated in the presence of ATPγS for a mutant Rca bearing the single-site substitution R294A.

In 2011, a bacterial red-type and two higher-plant green-type Rca X-ray structures became available, all demonstrating a classic AAA+ architecture.[28−30] For red-type Rca from *Rhodobacter sphaeroides* (Rs-Rca or CbbX), negative stain electron microscopy (EM) demonstrated the formation of ring-like hexamers in the presence of ATP and RuBP. In the absence of nucleotides, amorphous particles of ∼600−900 kDa were observed, whereas Mg·ATP without RuBP provided long fibers of ∼5−10 MDa.[28] Based on a mutational analysis of pore-lining residues, a model was proposed that involves the transient pulling of the Rubisco large subunit C-terminal peptide into the central pore of the Rs-Rca hexameric toroid, thereby facilitating release of inhibitory sugar phosphates.

Higher-plant Rca structures consist of the 1.9 Å resolution *Larrea tridentata* (creosote bush) substrate recognition domain, a helical bundle that forms the core of the AAA+ C-domain,[29] and the 2.9 Å resolution nucleotide-free *Nicotiana tabacum* (tobacco) core AAA+ module, which crystallized in a hexameric spiral subunit arrangement.[30] By EM, closed-ring hexamers were observed for the Nt-β-Rca-R294V variant in the presence of Mg·ATP or Mg·ATPγS (adenosine 5′-*O*-[γ-thio]-triphosphate), whereas Mg·ADP produced amorphous particles.[30] Mutational studies of central pore residues reduced or completely abolished Rubisco reactivation activity, again suggesting a role in peptide threading.[30] Although several Rca−Rubisco binding geometries have been proposed, the details of the physical interaction between these complexes await an explicit description.[31]

Despite the hexameric arrangements observed in EM images, mixing experiments of wild-type and mutant tobacco Rca led to the conclusion that three to six subunits are necessary for Rubisco activation. These data suggest that hexamerization may not be a strict requirement for function.[30] Using static light scattering (SLS), analytical ultracentrifugation (AUC), and small-angle X-ray scattering (SAXS) on tobacco Rca, Keown et al. arrived at an estimate of two to four subunits as the minimal requirement for both ATPase and Rubisco reactivation activities.[32] As in previous works, the apparent mass of apo-Rca was shown to increase continuously with increasing subunit concentration, with no apparent accumulation of particular intermediate forms.

To-date, experiments aimed at elucidating the mechanistic enzymology of Rca continue to be hampered by a lack of understanding of the mix of Rca complexes that coexists in solution under various conditions. Therefore, kinetic constants such as hydrolytic turnover numbers and Rubisco activation rates can only be interpreted as an average activity per Rca subunit.[33] Recently, we have developed fluorescence correlation spectroscopic (FCS) methods to determine individual binding constants for the stepwise assembly of cotton β-Rca.[34] FCS relies on the temporal fluctuation in fluorescence intensity that arises when a small number of molecules is present in an optically restricted volume.[35,36] Autocorrelation analysis relates these fluctuations to dynamic processes such as Brownian motion. For the first time, application of this method has allowed for the quantitative determination of the fractional population that each Rca oligomer presents at specific subunit concentrations in the presence of Mg·ADP.[34] In this work, the K_d values for Mg·ADP-mediated assembly were estimated to be 3.5 μM for the monomer−dimer equilibrium (K_{m-d}), 1 μM for the dimer−tetramer equilibrium (K_{d-t}), and 1 μM for the tetramer−hexamer equilibrium (K_{t-h}). The FCS results suggest that as much as four different oligomeric states coexist at cotton β-Rca concentrations typically used in ATPase and Rubisco reactivation kinetic assays.[33] Because self-association did not provide any plateaus under these conditions, the continued assembly to higher order states was modeled as a hexamer−24mer equilibrium (K_{h-24}) with a K_d value of 25 μM^3. Therefore, we have interpreted the ADP-mediated mechanism of assembly in terms of continued growth along a helical axis that is defined by an open spiral assembly,[34] in which each turn consists of six protomers as observed in the tobacco Rca crystal structure.[30] We have proposed that this mechanism is similar but not equal to the physiological assembly pathway, which likely involves closed-ring hexameric toroids.[34]

In the present work, we have applied the same FCS method to the investigation of cotton β-Rca assembly as a function of ligands that more closely mimic physiologically relevant conditions. To address the effects of different ATP levels in the chloroplast stroma, we have utilized the slowly hydrolyzing ATP analog ATPγS in oligomerization assays. We estimate that close to 80% hexamer can be generated *in vitro* over a narrow Rca concentration range. To confirm these results, we have investigated the early assembly steps of a substrate-trap mutant as a function of different ATP/ADP ratios. Notably, the data indicate the presence of a second Mg^{2+} binding site on the protein (in addition to the primary ATP-based coordination site) that appears to promote the formation of smaller oligomers at the expense of supramolecular aggregates.

MATERIALS AND METHODS

Site-Directed Mutagenesis. A modified version of the QuickChange method (Stratagene, Lo Jolla, CA) was used to introduce the D173N substitution into a *Gossypium hirsutum* (cotton) β-Rca harboring a C-terminal Ala-Cys insertion (Gh-

dx.doi.org/10.1021/bi500968h | *Biochemistry* XXXX, XXX, XXX−XXX

β-Rca-378AC). This construct, termed β-Rca-AC throughout the text, was previously cloned into a pET151-dTOPO expression plasmid.[34] The following forward and reverse oligonucleotide primers were ordered from Integrated DNA Technologies (Coralville, IA): 5′-CTCTTCATCAACAATCTCGACGCTGGAG-3′ and 5′-CTCCAGCGTCGAGATTGTTGATGAAGAG-3′. PfuTurbo DNA polymerase and 10× Pfu DNA polymerase reaction buffer were purchased from Agilent Technologies (Santa Clara, CA), dNTPs were purchased from Life Technologies (Grand Island, NY), and *Dpn*I restriction enzyme was purchased from New England Biolabs (Ipswich, MA). Thermal cycling, *Dpn*I digestion, and heat shock transformation into chemically competent Top10 *Escherichia coli* cells was carried out according to the QuickChange site-directed mutagenesis guidelines. Single colony transformants from overnight LB (Luria−Bertani) agar plates containing 100 μg/mL carbenicillin were cultured in 25 mL of LB with 100 μg/mL carbenicillin, and grown overnight at 37 °C and 250 rpm. After centrifugation (5000 rpm, 4 °C, 10 min), plasmids were purified from overnight cultures using the centrifugal method from the Qiagen Plasmid Mini Prep Kit (Germantown, MD). The correct mutation was confirmed by DNA sequencing.

Expression, Purification, and Dye Conjugation of Rca. β-Rca-AC and its variants were recombinantly expressed from pET151-dTOPO or pET23 plasmids, with and without N-terminal 6XHis affinity tags, respectively, as previously described.[34] β-Rca-AC expressed without an affinity tag was purified according to methods published earlier.[24] Nucleotides and other reagents used were of the highest purity reasonably obtainable. Frozen cell pellets (−80 °C) from 3 L of culture expressing β-Rca-AC or β-Rca-AC-D173N were thawed on ice and suspended in 50 mL of 25 mM Tris-HCl, pH 8.0, 10 mM imidazole, pH 8.0, 10% glycerol, ∼30 μM hen egg white lysozyme (Sigma-Aldrich), 1 mM phenylmethanesulfonylfluoride, 1 mM DTT, 0.1 mM ADP, and 0.1 mM EDTA, then stirred at 4 °C for 30 min and disrupted by sonication. Cell lysate was pelleted by centrifugation, and the supernatant was passed through a 0.8 μm syringe filter before being loaded onto a Ni^{2+}-nitrilotriacetic acid (Ni-NTA) column (Qiagen, Valencia, CA). Protein was purified using an imidazole buffer step gradient (25 mM Tris-HCl, pH 8.0, 500 mM NaCl, 1 mM DTT, and 0.1 mM ADP, plus variable amounts of imidazole). After the columns were washed with 10 and 80 mM imidazole buffer, His-tagged β-Rca-AC and β-Rca-AC-D173N were eluted from the column with 35 mL of 200 mM imidazole buffer. The pooled elution fractions were digested with tobacco etch virus (rTEV) protease to remove the 6XHis tag, dialyzed overnight, passed over a second Ni-NTA column and concentrated to 2.5 mL in Centriprep concentrators (Millipore, Milford, MA) as described.[34] Samples were then buffer exchanged into 25 mM HEPES−NaOH, pH 7.5, 250 mM KCl, 2 mM nucleotide (ADP, ATP, ATPγS, or AMP-PNP [5′-adenylyl-imidodiphosphate]), 5 mM $MgCl_2$ (or no $MgCl_2$), and 10% glycerol using PD-10 columns (GE Healthcare). Protein concentrations were determined using the Bradford method, with typical yields of 3−4 mg/L cell culture and 1.6 mg/L cell culture for β-Rca-AC and β-Rca-AC-D173N, respectively. β-Rca-AC and β-Rca-AC-D173N conjugation with an Alexa-546 C_5-maleimide fluorophore and analysis for efficiency of dye labeling followed the published method,[34] except that ALEXA dye stock was prepared at 350 μM in 50 mM HEPES−NaOH, pH 7.2, rather than at 1.93 mM in 50 mM Na_2HPO_4/NaH_2PO_4, pH 7.2.

HPLC and Spectrophotometric and Mass Spectrometric Analysis of Labeled Protein. Alexa-labeled β-Rca-AC and β-Rca-AC-D173N samples were analyzed by reverse-phase HPLC (Agilent Technologies 1260 Infinity Quaternary LC system, Agilent Technologies 1100 series diode-array detector) on a C18 analytical column (Phenomenex Prodigy, 5 μm ODS-3, 100 Å pore size, 250 mm × 4.6 mm) using a linear water/acetonitrile gradient with 0.1% trifluoroacetic acid (TFA). Protein was monitored by optical density (OD) at 220 and 280 nm, and Alexa dye was monitored by OD 550 nm. Whereas free Alexa eluted at 40.5 min, all protein eluted at 36.5 min. Protein fractions were collected by hand, and absorbance spectra measured using 50% acetonitrile, 0.1% TFA, as a blank. From these spectra, molar ratios for Alexa/protein were calculated using the previously described method.[34] To verify correct molecular mass of labeled samples, MALDI spectra were collected on a Voyager DE STR mass spectrometer as previously described.[34]

General FCS Sample Preparation Method. In typical FCS experiments, 500 μL of FCS sample buffer (25 mM HEPES, pH 7.6, 250 mM KCl, 2 mM nucleotide or nucleotide analog, 5 mM $MgCl_2$, and 10% glycerol) was placed on ice and used for sample dilutions. Protein preparations were buffer-exchanged into FCS sample buffer at Rca subunit concentrations of 85−90 μM for labeled and 110−135 μM for unlabeled protein. Subsequently, aliquots were flash-frozen with liquid nitrogen and stored at −80 °C. On the day of the FCS experiment, aliquots were thawed on ice, and both 1 and 10 μM stocks of unlabeled protein were prepared to be used in subsequent dilutions of labeled protein. All aliquots were kept on ice until measurement. For each experiment, appropriate amounts of labeled and unlabeled protein were mixed in siliconized low-retention microcentrifuge tubes containing 1× FCS sample buffer to give the desired final protein concentration. Regardless of total protein concentration, all samples were prepared so as to contain exactly 50 nM labeled protein. To allow subunit equilibration, samples ready for analysis were incubated for approximately 15 min on ice before performing FCS experiments.

For concentration-dependent experiments at different nucleotide ratios, aliquots of labeled and unlabeled β-Rca-AC-D173N containing either ATP or ADP were first mixed to give the desired nucleotide ratio, followed by dilution to the appropriate subunit concentration for the FCS measurement. For these experiments, the nucleotide content of the FCS buffers was adjusted to contain either 2.0 mM ATP, 1.5 mM ATP plus 0.5 mM ADP, or 2 mM ADP. For low $MgCl_2$ experiments, buffer contained 1.5 mM ATP, 0.5 mM ADP, and 2.02 mM $MgCl_2$.

FCS Sample Preparation for Mg^{2+} Titration Experiments at Fixed Protein Concentrations. A set of four FCS sample buffer solutions were prepared, each containing 1.5 mM ATP and 0.5 mM ADP with a differing total $MgCl_2$ concentration (1.7, 3, 5, or 7 mM). Samples for FCS containing 45 μM β-Rca-AC-D173N were prepared by mixing labeled protein with unlabeled protein following a dilution protocol analogous to the one described above. The concentration of free Mg^{2+} in solution was calculated assuming multiple equilibria and using the reported dissociation constants for ADP and ATP of 0.241 and 0.028 mM, respectively. Because the amount of ADP and ATP was fixed throughout the

dx.doi.org/10.1021/bi500968h | *Biochemistry* XXXX, XXX, XXX−XXX

experiment, this allowed the concentration of free Mg^{2+} in the final sample to be adjusted simply by diluting with the appropriate amounts of one of the four FCS sample buffers with variable $MgCl_2$.

FCS Sample Preparation for Nucleotide Titration Experiments at Fixed Protein Concentration. For this experiment, labeled and unlabeled protein stock solutions were prepared by mixing an appropriate amount of thawed β-Rca-AC-D173N in ATP or in ADP, following dilution protocols as described above. Each experiment contained a total of 60 μM β-Rca-AC-D173N, of which 50 nM was labeled. FCS sample buffers with differing nucleotide compositions were used to dilute protein samples to the desired final concentration of 60 μM. Nucleotide composition was 2 mM ATP, 1.5 mM ATP plus 0.5 mM ADP, 1 mM ATP plus 1 mM ADP, 0.5 mM ATP plus 1.5 mM ADP, and 2 mM ADP.

Fluorescence Fluctuation Spectroscopy Data Collection. FCS measurements were carried out using a home-built confocal optical setup. Excitation was achieved with a Compass 215M-10 532 nm CW laser (Coherent GmbH, Germany) attenuated to 50 μW to minimize triplet dynamics. The output of the laser was expanded, collimated, and directed via a dichroic lens into an Olympus PlanApo 100×/1.4 NA oil objective. Samples were placed into silicone perfusion chambers (Grace Biolabs, Bend, OR) pretreated with BSA to minimize Rca adsorption onto the cover glass. Fluorescence from samples was collected via the same objective, separated from excitation light through the dichroic lens, and reflected into a 50 μm pinhole. The emission was then focused into an avalanche photodiode detector (PerkinElmer Optoelectronics, SPCM-AQR14). A bandpass filter was used before the detector to minimize stray light (Omega 3RD560-620). The recorded fluorescence signal was autocorrelated in real time using an ALV 5000/EPP, ALV-GmbH, Langen, Germany.

FCS Data Analysis. The autocorrelation function of a single species that diffuses freely in solution is given by[35]

$$G(\tau) = G_0\left(1 + \frac{4D\tau}{r_0^2}\right)^{-1}\left(1 + \frac{4D\tau}{z_0^2}\right)^{-1/2}$$

where τ is the correlation lag time, G_0 is the amplitude of the decay, D is the diffusion coefficient of the diffusing particle, and r_0 and z_0 are the radial and axial semi-axes of the Gaussian confocal volume.

The instrument was calibrated daily by measuring the FCS decays of free TAMRA dye (D = 414 μm^2 s^{-1}) in buffer[37,38] and fitting the experimental decays using r_0 and z_0 as fitting parameters. The diffusion coefficient of Rca was determined by fitting the experimental FCS decays using the values of r_0 and z_0 measured on the same day. As shown in our previous work, solutions of Rca are in general polydisperse and therefore the diffusion coefficients obtained from the fits represent apparent values for a given mixture of oligomeric species. Data are presented as normalized ratios D_{app}/D_1, where D_1 is the diffusion coefficient of the monomer measured with a 50 nM Rca subunit concentration.

General Parameters of the Enzcheck Phosphate Assay. Inorganic phosphate (Pi) production was monitored with a UV 2401 PC Shimadzu spectrophotometer using the Enzcheck phosphate assay (Life Technologies).[39] This assay is a continuous enzyme-linked assay in which the substrate 2-amino-6-mercapto-7-methyl purine riboside (MESG, λ_{max} = 330 nm) is converted to ribose-1-phosphate and 2-amino-6-mercapto-7-methyl purine (λ_{max} = 360 nm) by purine nucleoside phosphorylase (PNP). The coupling enzyme PNP consumes phosphate during turnover, such that ATPase activity is reflected by an increase in absorbance at 360 nm.

The standard curve for the Enzcheck assay was prepared in the following manner. Reference and sample cells containing 1× Enzcheck reaction buffer (50 mM Tris-HCl, pH 7.5, 1 mM $MgCl_2$, and 0.1 mM NaN_3) supplemented with 55 mM HEPES, pH 8, 1.6 mM DTT, and 4 mM $MgCl_2$ were autozeroed at 360 nm. All concentrations provided refer to the final volume of 1.00 mL in the cuvette. MESG and PNP were added sequentially to the sample cuvette to provide a final concentration of 200 μM and 3 U/mL, respectively. The mixture was allowed to equilibrate for 30 s before starting the time scan. Once the absorbance signal stabilized, known concentrations of phosphate (P_i) standard (KH_2PO_4) were added and manually mixed with a cuvette mixer, and time scans were continued until signal saturation was reached. The final reaction volume was 1 mL for each measurement and is reflected in all concentrations given above. For each P_i concentration, initial and final OD 360 values were recorded, and the difference was plotted as a function of P_i concentration. A linear equation fit to these data represented the standard curve that was subsequently used to calculate the rate of P_i release upon Rca-catalyzed ATP hydrolysis.

Measurement of ATPase Activity of β-Rca-AC and β-Rca-AC-D173N Using the Enzcheck Assay. The ATPase activity of 5 μM Rca was assayed in buffer containing 4 mM ATP, 60 μM ADP, and 5 mM $MgCl_2$, and also in buffer containing 0.5 mM ATP, 60 μM ADP, and 5 mM $MgCl_2$. Each condition was measured in triplicate. For this assay, substrate ATP was prepared in 100 mM HEPES, pH 8.0, to avoid acid hydrolysis. Reference and sample cells were autozeroed as described above for the P_i standard curve. Next, 200 nmol of MESG, 5 nmol of Rca, and 3 units of PNP were added sequentially, and the mixture was equilibrated for 1 min to consume contaminating phosphate until a stable signal was obtained. The time scan was started, and after 1 min, substrate ATP (4 μmol) was added, the sample was mixed manually, and the time scan was continued for another 4 min. P_i contamination from ATP gives a significant signal even in the absence of Rca. Therefore, a blank experiment was performed, in which a buffer blank (25 mM HEPES, 300 mM KCl, 1 mM DTT, 2 mM ADP, and 10% glycerol) was added instead of Rca. A second control experiment consisted of the addition of 5 μM bovine serum albumin (BSA, Sigma-Aldrich) instead of Rca, with BSA suspended in 25 mM HEPES, 300 mM KCl, 1 mM DTT, 2 mM ADP, and 10% glycerol. To calculate initial rates, the time scan collected on a buffer blank was subtracted from Rca or BSA turnover scans. The data range chosen for initial rate calculation consisted of the steepest linear portion of the time scan, which was generally 20−30 s long. The corrected initial slope was converted to the rate of phosphate (P_i) production by use of the standard curve. The turnover rate of Rca was calculated by dividing the rate of change in phosphate concentration by the subunit concentration of Rca.

Measurement of ATP Hydrolysis during β-Rca-AC-D173N Preparation for FCS Experiments. The phosphate content of β-Rca-AC-D173N was determined under conditions identical to those used for FCS sample preparation. Frozen (−80 °C) aliquots of 113 μM protein in 25 mM HEPES−NaOH, pH 7.5, 250 mM KCl, 5 mM $MgCl_2$, 10% glycerol, and 2 mM ATP were thawed on ice, alongside corresponding buffer

dx.doi.org/10.1021/bi500968h | Biochemistry XXXX, XXX, XXX−XXX

samples. Protein solution (22.1 μL) was transferred to a cuvette containing 0.2 mM MESG, 3 units of PNP, 50 mM Tris, pH 8.0, 55 mM HEPES, pH 8.0, 1 mM $MgCl_2$, and 0.1 mM NaN_3, to provide a final volume of 1 mL in the cuvette. After mixing, the signal was allowed to stabilize, and the OD 360 was recorded. Buffer blanks were utilized for baseline correction, and the corrected OD 360 was utilized to determine the phosphate content in the sample using an appropriate standard curve (see above). Additional time points were collected upon protein incubation for 20, 175, and 300 min on ice. The phosphate content of the protein sample calculated from these data was assumed to result from ATP hydrolysis and therefore to be equivalent to the ADP content. Traces of phosphate arising from sources other than ATP hydrolysis were taken into account by the baseline correction method.

Measurement of ATPγS Hydrolysis during β-Rca-AC Preparation for FCS Experiments. A number of protein samples used for FCS contained the slowly hydrolyzing nucleotide analog ATPγS. To quantitate the extent of ATPγS hydrolysis during sample preparation for FCS experiments, a nicotinamide adenine dinucleotide (NADH) enzyme-linked assay was used to measure the ADP content.[40] Frozen (−80 °C) samples containing 5 mg/mL protein in 25 mM HEPES−NaOH, pH 7.5, 250 mM KCl, 5 mM $MgCl_2$, 10% glycerol, and 2 mM ATPγS were thawed on ice alongside corresponding buffer samples. Protein solution (25.5 μL) was added to a cuvette containing 0.3 mM NADH, 2 mM phoshoenolpyruvate, 100 mM tricine, pH 8.0, 5 mM $MgCl_2$, 20 mM KCl, 4.8−8 U of pyruvate kinase, and 7.2−11.2 U of lactate dehydrogenase, to provide a final volume of 1 mL. Blank measurements were recorded upon addition of 25.5 μL buffer. The signal at 340 nm was observed to decrease with time, then to stabilize to a constant value. The difference between the initial and final OD 340 readings, corrected by measurements on the buffer blank, was converted to the amount of NADH consumed by use of the NADH extinction coefficient (ε_{340}) of 6220 M^{-1} cm^{-1}.[41] This value was set equal to the amount of ADP produced by ATP hydrolysis. The measurement was repeated for ice incubation times of 20, 175, and 300 min.

Thermofluor Stability Assays. Fluorescence data were collected with an ABI Prism 7900HT sequence detection system (Applied Biosystems). β-Rca-AC and β-Rca-AC-D173N premixes at 1.05× were prepared as described previously,[24] and 19 μL of premix was pipetted into the wells of a 384-well polypropylene TempPlate PCR plate, which was kept on ice. Nucleotides (ADP, ATP, ATPγS, or AMP-PNP) at 2 mM, $MgCl_2$ at 5 mM, or both were introduced by addition of 1 μL stocks containing either 40 mM nucleotide, 100 mM $MgCl_2$, or both. For lower nucleotide or magnesium content, buffers were adjusted accordingly. Each individual well of the TempPlate PCR plate contained a final volume of 20 μL sample containing 0.25 mg/mL Rca, 25 mM HEPES−NaOH, pH 7.5, 150 mM KCl, 16× Sypro Orange (Invitrogen), and appropriate amounts of nucleotide and magnesium ions. Sypro Orange is supplied as a 5000× solution by the manufacturer. Each buffer condition was set up in triplicate. The plate was sealed with optically clear tape, and data were collected and processed as previously described.[24]

RESULTS

ATPγS Promotes Hexamerization of Cotton β-Rca-AC, while ADP Favors Larger Oligomers. To better understand nucleotide dependence of Rca subunit assembly, we have used previously developed FCS methods to monitor oligomerization in the presence of the slowly hydrolyzing ATP analog ATPγS and compared the results with the assembly process in the presence of ADP.[34] As described previously, a fluorescent label was attached to the Rca C-terminus by employing a carboxy-terminal Ala-Cys insertion variant originally derived from *Gossypium hirsutum* (cotton) short-form (β) Rca.[42] Here, this variant is termed β-Rca-AC and is also referred to as wild-type protein (loosely defined). This protein was expressed in *E. coli* as an N-terminally 6His-tagged fusion protein and purified by Ni-affinity chromatography. The tag was cleaved with rTEV (recombinant tobacco etch virus) protease, and the thiol-directed label AlexaFluor-546 was attached to the protein's engineered cysteine residue by means of maleimide chemistry.[34] We were able to efficiently incorporate one label per protomer for all reactions carried out in the presence of ATPγS, as previously demonstrated for ADP-containing samples.[34] Absorbance spectra collected on HPLC-purified and acid-denatured protein were consistent with a molar ratio of 1.1 (n = 1) labels per protein chain, as further supported by MALDI mass spectrometry (see Supplementary Figures S1 and S2, Supporting Information). Enzymatic assays monitoring ADP production were employed to determine the amount ATPγS hydrolyzed by β-Rca-AC under conditions mimicking sample preparation on the day of the FCS experiment (typically 5 h for the measurement of a full Rca concentration range; Table S1, Supporting Information). These data were utilized to calculate an average ATPγS/ADP ratio of 8 (range 7−11) to be present in Rca·ATPγS samples during FCS data collection (Figure 1A).

Unfortunately, similar experiments could not be carried out in the presence of the nonhydrolyzable ATP-analog AMP-PNP (β,γ-imidoadenosine 5′-triphosphate), because Rca·AMP-PNP MALDI spectra provided evidence for the incorporation of two labels per protein chain, suggesting that a normally buried native cysteine residue has become solvent-accessible. Thermal destabilization of β-Rca-AC due to AMP-PNP binding was further supported by Thermofluor assays as described below (Table 1). Therefore, FCS analysis of β-Rca-AC in the presence of AMP-PNP was not pursued further.

β-Rca-AC samples were prepared between 50 nM and 100 μM subunit concentration with each sample containing 50 nM dye-conjugated protein, 2 mM ATPγS, and 5 mM total $MgCl_2$ at pH 7.6. Control experiments indicated that mixing of labeled and unlabeled Rca preparations provided complete subunit equilibration within 10 min incubation on ice, in line with a random distribution of labeled and unlabeled subunits. Under these conditions, the free magnesium ion concentration, that is Mg^{2+} not coordinated to ATPγS, was estimated to be 3.02 mM based on its ATP-binding constant.[43] This compares to a free Mg^{2+} concentration of 3.14 mM in the presence of 2 mM ADP under otherwise identical conditions.

As described previously,[34] the autocorrelation function was utilized to calculate FCS decay curves from the fluorescence intensity fluctuations (Supplementary Figure S3, Supporting Information). These curves were fit to an apparent diffusion coefficient (D_{app}) that contains contributions from all oligomeric species present in the observation volume during measurement. At Rca subunit concentrations between 50 and 300 nM, the FCS decays of β-Rca-AC with Mg·ATPγS provide a relatively constant D_{app} (Figure 1A). Photon counting histogram (PCH) analysis confirmed that β-Rca-AC is monomeric over this concentration range, as demonstrated previously for Mg·ADP bound samples.[34] When the subunit

dx.doi.org/10.1021/bi500968h | *Biochemistry* XXXX, XXX, XXX−XXX

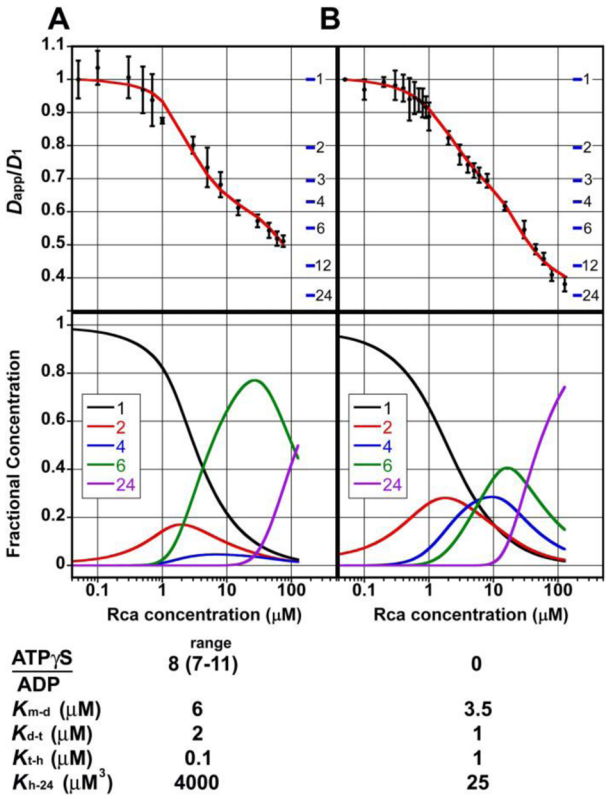

Figure 1. Assembly mechanism of β-Rca-AC as a function of ATPγS and ADP. (top) Relative apparent diffusion coefficients (D_{app}/D_1) of β-Rca-AC determined by FCS as a function of subunit concentration (black circles). Each sample was prepared in buffer containing 25 mM HEPES−NaOH, pH 7.6, 250 mM KCl, 5 mM $MgCl_2$, 10% glycerol, and 2 mM ATPγS (A) or 2 mM ADP (B). For panel A, the ATPγS/ADP ratio was estimated to be 8 (range 7−11) during FCS data collection. The data shown in panel B have been published previously[34] and are replotted for ease of comparison. The horizontal blue lines are placed at calculated values of D_{app}/D_1 for k = 1, 2, 3, 4, 6, 12, and 24, where k represents the number of subunits per assembly. The red curves represent computer simulations of the Rca assembly mechanism calculated using the K_d values shown in the table below. (bottom) Fractional concentrations of oligomeric species as a function of Rca subunit concentration, as calculated from the K_d values determined by manual curve fitting.

concentration was raised above 300 nM, the FCS decay curves shifted to longer time scales, indicating Rca oligomerization (Supplementary Figure S3, Supporting Information). Figure 1 presents a plot of the D_{app}/D_1 values (D_1 = $D_{monomer}$) as a function of total subunit concentration in the presence of Mg·ATPγS (panel A), compared with previously published data with Mg·ADP[34] (panel B). Although the two curves are very similar from 50 to 700 nM Rca, a steeper decrease in D_{app}/D_1 is observed between 0.7 and 15 μM with Mg·ATPγS than with Mg·ADP. This observation suggests that in the low-micromolar range, oligomer formation is promoted by ATPγS. Strikingly, the opposite trend is observed at concentrations ranging from 30 to 100 μM Rca, where continued assembly to higher-order aggregates appears to be attenuated by Mg·ATPγS compared with Mg·ADP (Figure 1).

To provide a theoretical scale for the expected diffusion coefficients for monodisperse β-Rca-AC, D_{app}/D_1 values were calculated from the molecular weight of pure monomeric, dimeric, trimeric, etc. species by assuming a spherical shape

Table 1. Thermofluor-Based Stability Data for β-Rca-AC as a Function of Nucleotide Analogs and Magnesium Ion Concentration[a]

ATPγS (mM)	AMP-PNP (mM)	Mg^{2+} (mM)	β-Rca-AC $T_{m\text{-}app}$ (°C ± SD)
			37.0 ± 0.6
		5	35.7 ± 0.4
0.01			37.8 ± 0.3
0.1			39.3 ± 0.3
1			43.1 ± 0.2
2			44.4 ± 0.2
4			45.4 ± 0.1
0.01		5	36.5 ± 0.1
0.1		5	38.9 ± 0.2
1		5	43.4 ± 0.2
2		5	44.5 ± 0.1
4		5	45.7 ± 0.2
	0.01		36.7 ± 0.3
	0.1		36.9 ± 0.2
	1		38.5 ± 0.4
	2		39.5 ± 0.2
	4		40.6 ± 0.3
	0.01	5	35.5 ± 0.1
	0.1	5	35.6 ± 0.1
	1	5	37.1 ± 0.2
	2	5	38.1 ± 0.2
	4	5	39.1 ± 0.3

[a]All data were collected in triplicate (n = 3).

(Figure 1, blue horizontal bars). As shown previously,[34] utilizing the radius of gyration of available X-ray models[30] instead of a spherical approximation did not modify the calculated diffusion coefficients substantially. To characterize the thermodynamics of Rca assembly, we employed a previously developed mathematical model that describes the total autocorrelation function in terms of individual contributions from each oligomeric species.[34] This analysis allows for the input of K_d values as variable parameters to simulate expected D_{app} values as a function of Rca concentration. As before, two assembly mechanisms were tested.[34] The first involved the concerted assembly of six monomers to form a hexamer, followed by association of four hexamers to form a 24-mer. The second involved the stepwise assembly of monomers to dimers, dimers to tetramers, tetramers to hexamers, and hexamers to 24-mers, thus requiring the input of four K_d values. In both models, the assembly state of 24 subunits was used as a placeholder for higher-order aggregates, because the FCS data cannot distinguish large species that differ by a few subunits (Figure 1). For each model, iterative rounds of K_d optimizations were carried out by systematically varying the input K_d values both one at a time and simultaneously, to arrive at predicted D_{app}/D_1 values that follow the experimental data closely.

As observed previously for Mg·ADP-mediated assembly,[34] the Mg·ATPγS data do not fit well to the concerted model. Therefore, species intermediate to monomers and hexamers must be explicitly modeled (Figure 1A, red curve). A good fit to the data is obtained with K_{m-d} = 6 μM for the monomer−dimer equilibrium, K_{d-t} = 2 μM for the dimer−tetramer equilibrium, K_{t-h} = 0.1 μM for the tetramer−hexamer equilibrium, and $K_{h-24} \approx$ 4000 μM^3 for the hexamer−24mer equilibrium. Iterative cycles of simulations varying the K_{m-d} and

dx.doi.org/10.1021/bi500968h | Biochemistry XXXX, XXX, XXX−XXX

K_{d-t} values suggest that these parameters are highly correlated but independent of K_{t-h} and K_{h-24}, which are poorly correlated to each other. In other words, a poor agreement between experiment and simulation upon choosing a particular K_{t-h} value cannot be compensated for by the systematic adjustment of K_{h-24}, nor vice versa.

A comparison of the K_{m-d} and K_{d-t} values extracted for ATPγS to those of the ADP-mediated assembly process suggests that the formation of dimers and tetramers may be slightly weaker with Mg·ATPγS than with Mg·ADP (6 and 2 μM vs 3.5 and 1 μM, see Figure 1). However, the significance of these differences is difficult to evaluate, because a rigorous error estimate is not available. Regardless, only the processes of hexamerization (K_{t-h}) and large aggregate formation (K_{h-24}) are significantly affected by the change in nucleotide (Figure 1). Formation of hexameric species appears substantially promoted by Mg·ATPγS, since the extracted K_{t-h} value of 0.1 μM is 10-fold smaller than that for Mg·ADP (1 μM). At the same time, assembly to very large aggregates is substantially disfavored in the presence of Mg·ATPγS, as indicated by a K_{h-24} value of about 4000 μM^3 compared with only 25 μM^3 for Mg·ADP.

The extracted K_d values were utilized to calculate fractional concentrations of assembly intermediates as a function of concentration (Figure 1, lower panels). Between 1 and 4 μM β-Rca-AC, our model predicts 15−18% dimeric species in the presence of Mg·ATPγS, somewhat less than the 26−28% predicted for Mg·ADP. However, between 8 and 70 μM, about 60−80% hexameric species are predicted for Mg·ATPγS. Under these conditions, the hexameric component reaches a maximum of 76% at 30 μM β-Rca-AC subunit concentration. These values are significantly higher than the 30−40% hexamer predicted for Mg·ADP over a similar concentration range. However, at 100 μM β-Rca-AC, our model predicts only 40% high-MW aggregates for Mg·ATPγS, whereas ADP provides for 70% aggregates. In combination, our data clearly indicate that Mg·ATPγS stabilizes the formation of hexameric species, whereas Mg·ADP disfavors hexamers and enhances the formation of larger complexes.

Hydrolysis-Deficient β-Rca-AC-D173N Binds Nucleotides and Assembles Like Wild-Type in a Nucleotide-Dependent Fashion. To account for any assembly artifacts due to the substrate analog ATPγS, control experiments were carried out using the natural substrate ATP in combination with the mutant protein β-Rca-AC-D173N. In this variant, Walker-B Asp173 (CLFIND), predicted to be the catalytic base in ATP hydrolysis by sequence homology,[16] is replaced by an asparagine residue. Labeling of β-Rca-AC-D173N with AlexaFluor-546 in ATP-containing buffer provided molar ratios of 1.1 ± 0.1 (n = 2) covalently attached fluorophores per chain. Similarly, in ADP-containing buffers, molar ratios of 0.9 ± 0.1 (n = 3) were determined by use of all analytical methods described above (see also Supplementary Figures S1 and S2, Supporting Information). Therefore, this variant was judged to be suitable for FCS studies.

As a first step, ADP-mediated assembly of β-Rca-AC-D173N was compared with that of its parent protein[34] (Figure 2). Although D_{app}/D_1 displayed larger standard deviations for the mutant than those typically observed for wild-type, assembly appeared to proceed in nearly identical fashion. Optimization of K_d values using the algorithm described previously provided binding constants within experimental error of those obtained for the wild-type protein (Figure 2, bottom). For β-Rca-AC-D173N with Mg·ADP, the extracted values for K_{m-d}, K_{d-t}, K_{t-h}, and K_{h-24} were 6 μM, 0.5 μM, 0.5 μM, and 5 μM^3, respectively, which compares with 3.5 μM, 1 μM, 1 μM, and 25 μM^3 for β-Rca-AC (Figure 2).[34] In both cases, the fractional hexamer content appears to reach a maximum at 10−15 μM Rca, where it comprises about 40% of all subunits. These results imply that the assembly mechanism is not altered due to the D173N substitution, at least not within the limits of interpretation imposed by the rather noisy FCS data.

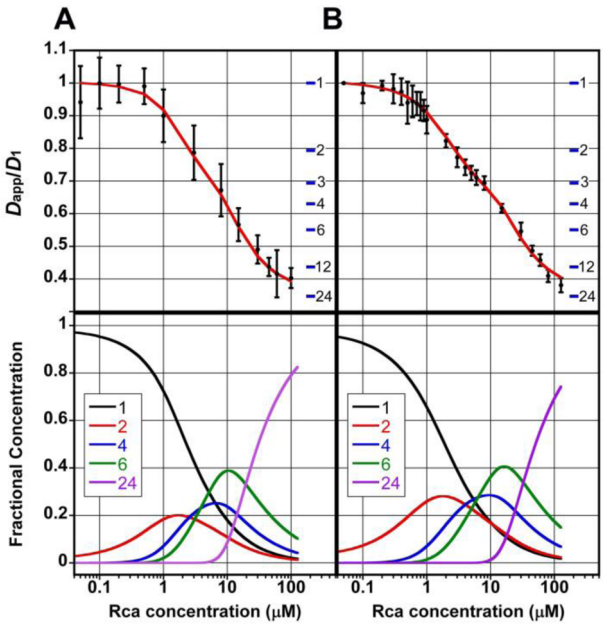

	D173N + ADP	WT + ADP
K_{m-d} (μM)	6	3.5
K_{d-t} (μM)	0.5	1
K_{t-h} (μM)	0.5	1
K_{h-24} (μM^3)	5	25

Figure 2. Comparison of the assembly mechanism of β-Rca-AC and β-Rca-AC-D173N protein in the presence of Mg·ADP. (top) Relative apparent diffusion coefficients (D_{app}/D_1) determined by FCS as a function of subunit concentration (black circles). Each sample was prepared in buffer containing 25 mM HEPES−NaOH, pH 7.6, 250 mM KCl, 5 mM $MgCl_2$, 10% glycerol, and 2 mM ADP: (A) β-Rca-AC-D173N; (B) β-Rca-AC. The data shown in panel B have been published previously[34] and are replotted for ease of comparison. The horizontal blue lines are placed at calculated values of D_{app}/D_1 for k = 1, 2, 3, 4, 6, 12, and 24, where k represents the number of subunits per assembly. The red curves represent computer simulations of the assembly mechanism calculated using the K_d values shown in the table below. (bottom) Fractional concentrations of oligomeric species as a function of Rca subunit concentration, as calculated from the K_d values determined by manual curve fitting.

Second, we tested whether elevated ATP would favor smaller oligomeric states as observed for the wild-type protein. To this end, β-Rca-AC-D173N samples were prepared in buffers containing three different ATP/ADP ratios at a total nucleotide concentration of 2 mM and a total Mg^{2+} concentration of 5 mM (free Mg^{2+} = 3.0−3.1 mM). Surprisingly, ATPase assays carried out in parallel suggested residual ATP hydrolytic activity of the mutant protein. Therefore, kinetic assays were set up on ice to exactly mimic the sample preparation conditions employed for FCS experiments and used to estimate the average ATP/ADP ratio present in protein samples during FCS data collection (Supplementary Table S1, Supporting Information). In this way, ratios of 3.6 (range 3−6), 2.3 (range 2−3), and 0 (all ADP) were determined to accurately describe the

dx.doi.org/10.1021/bi500968h | Biochemistry XXXX, XXX, XXX−XXX

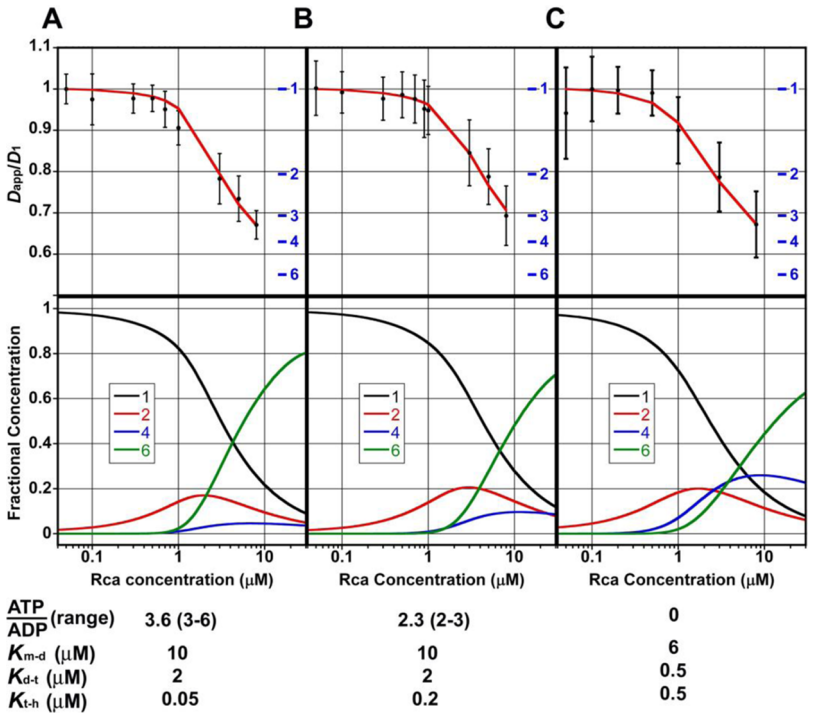

Figure 3. Assembly mechanism of β-Rca-AC-D173N as a function of the ATP/ADP ratio. (top) Relative apparent diffusion coefficients (D_{app}/D_1) determined by FCS as a function of subunit concentration (black circles). Each sample was prepared in buffer containing 25 mM HEPES, pH 7.6, 250 mM KCl, 5 mM $MgCl_2$, 10% glycerol, and 2 mM total nucleotide prepared at ratios of (A) ATP/ADP ≈ 3.6, (B) ATP/ADP ≈ 2.3, and (C) all ADP. The horizontal blue lines are placed at calculated values of D_{app}/D_1 for k = 1, 2, 3, 4, 6, 12, and 24, where k represents the number of subunits per assembly. The red curves represent computer simulations of the Rca assembly mechanism calculated using the K_d values shown in the table below. (bottom) Fractional concentrations of oligomeric species as a function of β-Rca-AC-D173N subunit concentration, as calculated from the K_d values determined by manual curve fitting. Note for panels A and B estimated average ATP/ADP ratios of 3.6 (range 3−6) and 2.3 (range 2−3) are reported based on the measured kinetics of ATP hydrolysis during sample preparation.

three types of conditions examined (Figure 3). Computer simulations of D_{app}/D_1 versus protein concentration between 50 nM and 8 μM yielded K_{m-d} values ranging from 6 to 10 μM, and K_{d-t} values ranging from 0.5 to 2 μM for the three ATP/ADP ratios. For both the monomer−dimer and the dimer−tetramer equilibrium, the all-ADP condition provided the smallest K_d values, again suggesting that ADP may promote a slightly increased propensity toward dimer and tetramer formation (Figure 3). Although this effect is consistent with the data collected on β-Rca-AC (Figures 1 and 2), the differences are rather subtle and difficult to quantitate. In contrast, extracted K_{t-h} values for the formation of hexamers exhibited strong ATP-dependence. These values were 0.05, 0.2, and 0.5 μM for high, medium, and low ATP, respectively, revealing increasingly tight hexamerization with increasing ATP/ADP ratios (Figure 3). As observed for the wild-type protein (Figure 1), the estimated binding constant for hexamer formation differed by 1 order of magnitude between the high and low ATP conditions. The fractional concentrations of oligomeric species calculated from the optimized K_d values suggest that the maximum hexamer content is about 80%, 70%, and 60% at the respective ATP/ADP ratios of 3.6, 2.3, and 0. In combination, these data provide strong support for our findings for the assembly process of β-Rca-AC in the presence of ATPγS (Figure 1).

To further examine the effect of nucleotide ratio on assembly, we carried out FCS experiments at constant protein concentration of 60 μM β-Rca-AC-D173N while varying the nucleotide ratio. As before, samples were prepared at 2 mM total nucleotide and 5 mM total Mg^{2+} (free Mg^{2+} = 3.0−3.1 mM), but at five different ATP/ADP ratios that consisted of all-ATP, 3:1, 1:1, 1:3, and all-ADP (Figure 4A). At high ATP, β-Rca-AC-D173N demonstrated a large diffusion coefficient consistent with smaller assemblies of 6−12 subunits. Upon reduction of the ATP content, a slow and gradual decrease in D_{app} is observed, indicating the formation of somewhat larger species, such as dodecamers at an ATP/ADP ratio of 1/3. However, when ATP is removed completely, a steep drop of D_{app}/D_1 is observed, in line with high-MW aggregate formation significantly larger than a dodecamer. These findings agree with all protein concentration-dependent studies presented above on β-Rca-AC (Figures 1 and 2), confirming that smaller oligomers are favored at higher ATP/ADP ratios.

Free Mg^{2+} Promotes Hexamer-Like Oligomeric Forms of β-Rca-AC-D173N. To assess whether excess Mg^{2+} affects the Rca assembly process, we used FCS to determine the D_{app} of preparations containing 45 μM β-Rca-AC-D173N in the presence of 2 mM total nucleotide. For this experiment, the ratio of ATP/ADP was kept constant at 3:1, whereas the concentration of total Mg^{2+} was adjusted to provide free Mg^{2+} concentrations (i.e., not coordinated to ATP or ADP) between 0.1 and 5 mM (Figure 4B). Strikingly, the value of D_{app}/D_1 increased substantially with increasing free Mg^{2+}, rising from 0.47 at 0.1 mM free Mg^{2+} to 0.53 at 5 mM free Mg^{2+}. A D_{app}/D_1 value of 0.53 equals the value for a heptameric species as calculated from its MW and lies within experimental error of the value of 0.55 calculated for a hexameric species (blue bars in Figure 4). Although 6- and 7-fold stoichiometries cannot be

dx.doi.org/10.1021/bi500968h | Biochemistry XXXX, XXX, XXX−XXX

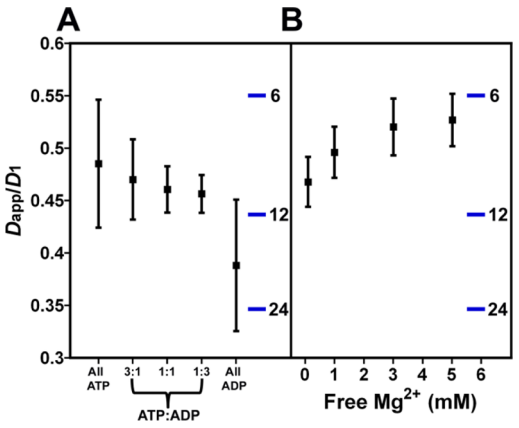

Figure 4. (A) Formation of supramolecular assemblies of 60 μM β-Rca-AC-D173N with decreasing ATP/ADP ratios. Apparent (D_{app}) and normalized diffusion coefficients (D_{app}/D_1) were determined in the presence of different nucleotide ratios as indicated, while keeping the protein concentration constant. The error bars represent the standard deviations of at least three independent measurements. (B) Disassembly of 45 μM β-Rca-AC-D173N with increasing free Mg^{2+} concentrations. Apparent (D_{app}) and normalized diffusion coefficients (D_{app}/D_1) were determined in the presence of 1.5 mM ATP and 0.5 mM ADP (ATP/ADP = 3:1). The total Mg^{2+} concentration was utilized to calculate free Mg^{2+}, that is, Mg^{2+} not coordinated to nucleotide. The error bars represent standard deviations of experiments carried out in triplicate.

distinguished experimentally by FCS, results obtained for the parent protein at the same concentration (45 μM) provide a similar D_{app}/D_1 ratio. For the parent protein, we have interpreted this ratio as representing 70% hexamer and 15% larger aggregates (Figure 1), in support of the promotion of hexamer formation by free magnesium ions. Notably, the magnesium effect exhibits saturation behavior at concentrations above 3 mM, suggesting specific binding to Rca assemblies in a manner that leads to dissociation of supramolecular aggregates in favor of hexamers. Therefore, Mg^{2+} not only is a cofactor facilitating ATP binding and hydrolysis but also plays a critical role in mediating the formation of proper subunit contacts, possibly by coordination of acidic groups donated by adjacent chains. We propose that magnesium mediates the assembly of physiologically relevant self-association states.

Thermostability of β-Rca-AC and D173N as a Function of Nucleotides and Mg^{2+}. We hope that, ultimately, a microscopic understanding of Rca assembly states will allow for the design of appropriate studies to characterize the ATPase and Rubisco reactivation activities of functional oligomeric states, as well as examine their 3D structures. In light of the experimental difficulties encountered with the D173N variant, a detailed biophysical characterization of wild-type and substrate-trap variants appears critical not only for the interpretation of FCS data presented here but also for the design of future experiments. Therefore, the thermostabilities of cotton β-Rca-AC and its D173N variant were examined as a function of substrate analogs and divalent cations. To this end, the Thermofluor assay was employed, an assay that reports on protein unfolding by use of a solvatochromic dye present in solution.[44] As proteins expose their hydrophobic cores with rising temperature, an increase in fluorescence is induced, allowing for the estimation of the midpoint temperature for protein denaturation ($T_{m\text{-}app}$). Although the extracted $T_{m\text{-}app}$ cannot be considered a thermodynamic quantity, these values allow for the rapid examination of relative stabilities of different expression constructs in different buffer conditions.[24]

First, the ATP analogues ATPγS and AMP-PNP were tested for their interaction with β-Rca-AC at 2 mM nucleotide (Table 1). Although both analogs were observed to bind Rca, thermal stabilization by ATPγS was substantially more pronounced than stabilization by AMP-PNP, based on the respective $\Delta T_{m\text{-}app}$ values of 44.4 ± 0.2 °C and 39.5 ± 0.3 °C. ATPγS also provided larger thermal stabilization than ATP ($T_{m\text{-}app}$ = 40.3 ± 0.2 °C). These data imply that ATPγS binds more tightly than ATP to the Rca active site and that AMP-PNP destabilizes the protein fold compared with ATP. Surprisingly, the addition of Mg^{2+} to ATPγS samples did not modify the $T_{m\text{-}app}$ values to any extent, and the addition of Mg^{2+} to AMP-PNP samples led to further destabilization by about 1.4 °C (Table 1). We conclude that the thermal stabilization previously reported for the addition of Mg^{2+} to ATP-bound Rca is not mimicked by the two ATP analogs ATPγS and AMP-PNP, suggesting electrostatic or structural alterations in the active-site pocket.[24] Although ATPγS does not appear to modify subunit assembly (Figure 1), AMP-PNP could not be utilized in FCS experiments (see above).

Second, we examined the thermostability of β-Rca-AC-D173N and compared the values to its parent protein (Table 2). In the absence of nucleotides and Mg^{2+}, the $T_{m\text{-}app}$ value of D173N was shown to be 34.5 ± 0.4 °C, somewhat depressed from the β-Rca-AC value of 37.0 ± 0.6 °C,[24] in line with fold destabilization. As with the parent protein, titration of D173N with adenine nucleotide provided an incremental increase in melting temperature, confirming nucleotide binding. Saturation with ADP was shown to raise the $T_{m\text{-}app}$ substantially to 47.5 ± 0.4 °C, only slightly below the value of 48.2 ± 0.1 °C obtained for the parent (Table 2). The more substantial rise in $T_{m\text{-}app}$ observed for the mutant ($\Delta T_{m\text{-}app}$ = 13 °C) compared with the parent ($\Delta T_{m\text{-}app}$ = 11 °C) implies stronger ADP binding to D173N. Interestingly, the most stable condition for both β-Rca-AC and β-Rca-AC-D173N appears to be 8 mM ADP in the absence of Mg^{2+} ($T_{m\text{-}app}$ = 48.2 and 47.5 °C, respectively).

When 1 mM free Mg^{2+} was added to 8 mM ADP, the $T_{m\text{-}app}$ decreased for both β-Rca-AC and D173N by 2.7 and 1.2 °C, respectively (Table 2). However, 1 mM free Mg^{2+} did not affect either of the two apo-proteins; as much as 9 mM free Mg^{2+} was necessary to observe a moderate loss of stability (~1.2 °C). At conditions mimicking the FCS experiments (Figure 2), that is, 2 mM ADP with 3 mM free Mg^{2+}, the melting temperatures of 42.7 °C (β-Rca-AC) and 42.3 °C (β-Rca-AC-D173N) indicated essentially identical stabilities for both proteins. Therefore, the larger uncertainties in diffusion coefficients measured for D173N may be a consequence of its propensity to aggregate (Figure 2).

For both proteins, ADP was shown to be more stabilizing than ATP (Table 2). However, this stabilization appeared less pronounced for the mutant ($\Delta T_{m\text{-}app}$ = 4.8 °C) than for the parent protein ($\Delta T_{m\text{-}app}$ = 7.6 °C).[24] At 2 mM ATP and ~1 mM free Mg^{2+} (3 mM total Mg^{2+}), the mutant exhibited a $T_{m\text{-}app}$ value of only 43.8 ± 0.3 °C, compared with 45.6 ± 0.2 °C for the parent protein. In the absence of Mg^{2+}, the data suggest stronger ATP binding to D173N, likely due to a net reduction in active-site negative charge density that would electrostatically repel the substrate triphosphate tail. In support of electrostatic arguments, addition of Mg^{2+} to ATP stabilizes the wild-type protein ($\Delta T_{m\text{-}app}$ = 4.1 °C) but does not provide stabilization of the mutant protein (Table 2).

dx.doi.org/10.1021/bi500968h | *Biochemistry* XXXX, XXX, XXX–XXX

Table 2. Thermofluor-Based Stability Data Comparing β-Rca-AC and β-Rca-AC-D173N as a Function of Substrate and Product Nucleotide, and Magnesium Ion Concentrations[a]

			$T_{m\text{-}app}$ (°C ± SD)	
ADP (mM)	ATP (mM)	Mg^{2+} (mM)	β-Rca-AC	β-Rca-AC-D173N
0			37.0 ± 0.3	34.5 ± 0.3
0.01			38.4 ± 0.2	36.0 ± 0.1
0.1			41.0 ± 0.2	40.0 ± 0.4
1			45.2 ± 0.1	44.9 ± 0.4
2			46.0 ± 0.2	45.4 ± 0.1
4			47.2 ± 1.1	46.3 ± 0.2
8			48.2 ± 0.1	47.5 ± 0.4
0		0	37.0 ± 0.6	34.5 ± 0.4
1		2	44.5 ± 0.1	44.5 ± 0.1
2		3	42.7 ± 0.2	42.3 ± 0.1
4		5	46.2 ± 0.3	46.6 ± 0.7
8		9	45.5 ± 0.4	46.3 ± 0.1
	0		37.0 ± 0.6	34.5 ± 0.4
	0.01		37.1 ± 0.6	36.9 ± 0.4
	0.1		38.4 ± 0.2	40.9 ± 0.1
	1		40.2 ± 0.2	43.6 ± 0.4
	2		40.2 ± 0.5	44.0 ± 0.2
	4		41.3 ± 0.1	44.2 ± 0.4
	8		40.6 ± 0.1	42.7 ± 0.2
	0	0	37.0 ± 0.6	34.5 ± 0.4
	1	2	45.8 ± 0.1	44.2 ± 0.2
	2	3	45.6 ± 0.2	43.8 ± 0.3
	4	5	45.0 ± 0.5	43.4 ± 0.1
	8	9	44.7 ± 0.2	42.8 ± 0.6
		0	36.7 ± 0.1	34.5 ± 0.4
		1	36.5 ± 0.3	34.8 ± 0.3
		2	35.7 ± 1.1	34.5 ± 0.7
		3	35.7 ± 0.6	33.6 ± 0.4
		5	35.4 ± 0.5	33.6 ± 0.8
		9	35.4 ± 0.1	33.3 ± 0.4

[a]All data were collected in triplicate (n = 3).

Residual ATPase Activity of β-Rca-AC-D173N Compared with β-Rca-AC. Although numerous studies on AAA+ proteins have been reported with "substrate-trap" mutants that lack the catalytic base,[11,45−50] a low level of ATPase activity was observed for β-Rca-AC-D173N (Supplementary Table S2, Supporting Information). This result was surprising, because previous work on tobacco Rca-D174Q and Rca-D174A did not provide any evidence of ATPase activity.[51] To be able to interpret FCS data appropriately, we analyzed the ATPase activity of this variant in relation to that of its parent protein by monitoring phosphate production at room temperature via the EnzCheck assay.[39] At 0.5 and 4 mM ATP, the activity of β-Rca-AC-D173N was observed to be 4- and 13-fold lower than that of the parent protein, whereas bovine serum albumin (BSA) exhibited about 15-fold lower activity (Supplementary Table S2, Supporting Information). Since the turnover rates of β-Rca-AC-D173N and BSA were less than one reaction per minute and exhibited a relative standard deviation of 50−70%, the residual activity of β-Rca-AC-D173N cannot be distinguished from the nonspecific ATPase activity of BSA. These results suggest nonspecific but protein-mediated substrate hydrolysis (all data corrected for ATP hydrolysis in the absence of protein).

To measure the reduction of the ATP/ADP ratio during sample incubation on ice, substrate hydrolysis was assayed at specific time points over a period of 300 min. For β-Rca-AC-D173N, the EnzCheck assay was utilized to determine the degree of ATP hydrolysis (Supplementary Table S1, Supporting Information),[39] whereas for β-Rca-AC, an enzyme-linked assay that follows NADH consumption was utilized to determine the degree of ATPγS hydrolysis.[40] Surprisingly, ATPγS hydrolysis by the parent protein proceeded significantly more slowly than ATP hydrolysis by β-Rca-AC-D173N. For this reason, we were able to collect FCS data on β-Rca-AC (Figure 1) at ATPγS/ADP ratios substantially higher than the ATP/ADP ratios that were achievable for the mutant protein (Figure 3). In separate assays, we determined that the level of ADP contamination in commercially available ATPγS samples is 3.1−3.4%, whereas the ADP contamination in commercially available ATP samples is only 0.36−0.42%. Overall, we conclude that ATPγS-bound β-Rca-AC is more suitable than ATP-bound β-Rca-AC-D173N to address the effects of substrate binding on biophysical behavior, despite the relatively large amount of ADP contamination present in ATPγS preparations.

DISCUSSION

Nature often carries out complex biochemical tasks required for cellular homeostasis with the help of macromolecular assemblies that can be extensively regulated.[52,53] However, when a protein forms a continuum of self-associated states with subunits that undergo rapid exchange, it becomes increasingly difficult to relate functional data to subunit stoichiometry. Frequently, the exact nature of active oligomeric states and the fractional concentration of these species remain unknown. In AAA+ proteins, hexameric assemblies have been linked to the mechanical remodeling of macromolecular substrates. In addition, experiments on a variety of AAA+ proteins have demonstrated that coupling of ATPase activity with mechanical work is not obligatory[54] and can be up- or down-regulated by assembly to higher-order states or by binding to partner proteins.[55] Both sequential and probabilistic models for subunit conformational change have been proposed and are thought to involve large-scale structural rearrangements of hexameric rings due to hinge bending motions near the active sites of individual chains. For example, ClpX crystal structures have provided evidence that multiple conformational states can be accessed by individual subunits, with each involving an ensemble of subpopulations.[54] These features complicate a clear definition of biological activity of each microscopic state. To begin to address biological functionality in terms of partner protein remodeling, the microscopic equilibria of coexisting quaternary structures must be well-understood.

Cotton Short-Form Rca Forms 70−80% Hexamers at 4−8-fold Excess of ATP or ATPγS over ADP. Building upon previously established FCS methods,[34] we have characterized the effects of ATP, ATPγS, and free Mg^{2+} on the assembly equilibria of cotton short-form β-Rca. Unique to this method is the mathematical framework developed for modeling the thermodynamics of self-association with the explicit inclusion of populated intermediate states. Our work on cotton β-Rca-AC indicates that at low subunit concentrations ranging from 700 nM to 30 μM, the presence of the slowly hydrolyzing ATP analog ATPγS provides larger oligomeric species than the presence of ADP (Figure 1). When ATPγS is used, the hexameric form appears to be the dominant species between 4

dx.doi.org/10.1021/bi500968h | Biochemistry XXXX, XXX, XXX−XXX

Table 3. Summary of Estimated Equilibrium Constants[a]

ATP(γS)/ADP	~8:1		~4:1		~2:1		0:1	
	WT	D173N	WT	D173N	WT	D173N	WT	D173N
K_{m-d} (μM)	6		10		10		3.5	6
K_{d-t} (μM)	2		2		2		1	0.5
K_{t-h} (μM)	0.1		0.05		0.2		1	0.5
K_{h-24} (μM^3)	4000						25	5

[a]WT (wild-type) refers to cotton β-Rca-AC, and D173N refers to cotton β-Rca-AC-D173N.

and 100 μM with a maximum at 30 μM, where ~76% of subunits are predicted to be hexameric. The modeling of states intermediate to the monomeric and hexameric forms was necessary to provide a good fit to the FCS data, suggesting that the dimeric and tetrameric species are well-populated. When the subunit concentration is raised well above 30 μM, ATPγS appears to reduce the contribution of large aggregates in comparison to ADP. This feature indicates that at higher concentrations, ATPγS promotes the formation of hexameric forms as well. For clarity, a summary of all estimated equilibrium constants is presented in Table 3.

Additional experiments carried out with the substrate-trap mutant β-Rca-AC-D173N provided an independent confirmation of the results obtained with wild-type protein. As with β-Rca-AC, D173N preparations with ATP/ADP ratios of 3.6, 2.3, and 0 led to the prediction of a hexamer peak at ~30 μM subunit concentration. The different nucleotide ratios provided ~80%, ~70%, and ~60% hexamer content, respectively (Figure 3), suggesting that ATP/ADP ratios above about four may yield maximum hexamer content in *in vitro* assays (Table 3). Unfortunately, β-Rca-AC-D173N appeared somewhat destabilized relative to its parent protein (Table 2) and demonstrated residual hydrolytic activity at a rate somewhat faster than the hydrolysis of ATPγS catalyzed by β-Rca-AC (Tables S1 and S2, Supporting Information). Although the affinity for ADP appeared unmodified, D173N appeared to bind ATP more tightly with and without excess magnesium ions, reflecting the reduction in negative charge in the binding pocket (Table 2). The larger error estimates obtained for the mutant D_{app}/D_1 values (Figure 2) indicate an increased tendency toward aggregation, as was also observed during protein purification procedures. Therefore, work with D173N was not pursued further, and averaging of wild-type and mutant K_d values does not appear to be warranted. Therefore, the most reliable dissociation constants may be found in Figure 1 and the wild-type columns in Table 3.

Although many AAA+ proteins such as ClpX and ClpA form tightly bound stable hexameric toroids under most conditions,[13,47] a recent study on Vps4 demonstrated that fast-exchanging dimer−hexamer equilibria occur over a broad concentration range of 10−200 μM.[48] Although this observation appears reminiscent of Rca, Vps4 hexamers are more readily formed with ADP than with ATP, an effect opposite to that observed with Rca. The Vps4 dimer−hexamer K_d value was shown to be 3.7 nM^2 in the presence of ATP and 0.04 nM^2 in the presence of ADP. However, not all Vps4 states observed *in vitro* are thought to be physiologically relevant. For example, a small fraction of larger aggregates was reported to form above ~60 μM. In addition, the replacement of the Walker B catalytic glutamate has been shown to promote hexameric ring stacking yielding a dodecamer, again an assembly state that is not likely sampled *in vivo*.[48] Similarly, we propose that the high-MW aggregates observed for Rca·ADP, and to a lesser extent for Rca·ATPγS, may not be biologically relevant states (see below).

The Hexamerization K_d Values Suggest That Closed-Ring Toroidal Structures May Be Promoted at High ATP/ADP Ratios at the Expense of Helical Arrangements. In previous work, we proposed a model for β-Rca-AC assembly that consists of three distinct microscopic steps leading to hexameric forms, followed by the formation of larger complexes of ~24 subunits, best modeled as a single step (Figure 5).[34]

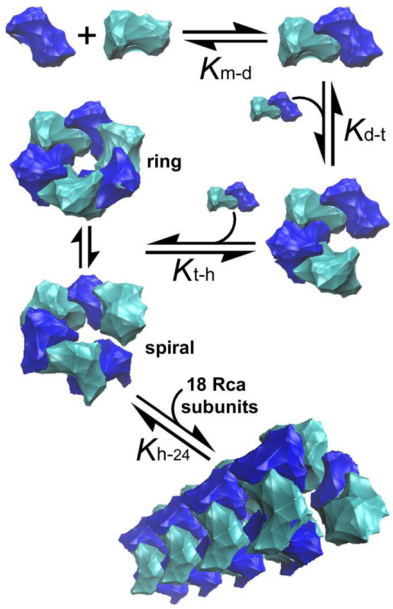

Figure 5. Schematic representation of the proposed Rca assembly model. Individual chains of the Rca AAA+ domain are shown in light and dark blue. K_{m-d}, monomer−dimer dissociation constant (K_d); K_{d-t}, dimer−tetramer K_d; K_{t-h}, tetramer−hexamer K_d; and K_{h-24}, hexamer−24mer K_d value. According to this model, dimeric and tetrameric oligomers assemble to form hexameric species. Two different kinds of assemblies consisting of six subunits each are proposed to be generated *in vitro*, a closed-ring and open-spiral form. The relative populations of each hexamer type are proposed to depend on nucleotide and magnesium conditions, and the experimentally determined K_{t-h} value is thought to reflect the relative contributions of each species (lower K_{t-h} indicates more pronounced closed-ring hexamer formation). The figure was generated by calculation of a coarse surface of the crystal structure of the AAA+ domain of tobacco Rca (PDB ID code 3T15), using the program Pymol.

Work presented here demonstrates that the monomer−dimer and dimer−tetramer equilibria exhibit only weak dependence on the ATP/ADP ratio, with K_{m-d} estimated to be 3 and 6 μM and K_{d-t} estimated to be 1 and 2 μM, in the absence and presence of ATPγS, respectively (Figure 1 and Table 3). However, substantial differences are observed for hexamer formation, since the K_{t-h} appears to be 10-fold lower in the

dx.doi.org/10.1021/bi500968h | *Biochemistry* XXXX, XXX, XXX−XXX

presence of ATPγS compared with ADP alone, dropping from 1 to 0.1 μM. Since the thermodynamics of hexamerization seems to exhibit a strong dependence on nucleotide, we propose a model in which ATP facilitates the formation of a closed-ring hexameric toroid, whereas ADP facilitates formation of an open hexameric spiral (Figure 5). An optimization of subunit interactions in the presence of ATP is consistent with the expectation that the binding of a dimer to a tetramer would bury twice the exposed molecular surface area if the ensuing ring forms a closed toroid rather than an open spiral. We suggest that the lower K_d value reflects the ATP-mediated preference of a doughnut-like arrangement of subunits that would be enthalpically more favorable. On the other hand, in the presence of ADP, the identical K_{d-t} and K_{t-h} values of 1 μM may reflect the energetically equivalent addition of a dimer to either another dimer or a tetramer to form an open spiral arrangement with potential subunit contacts unsatisfied. Therefore, the observed difference in K_{t-h} values for hexamer formation is consistent with the notion of two competing pathways, such as the parallel formation of both open and closed hexamers. The extracted binding constants likely reflect the relative contributions of each pathway. If this model is correct, the K_{t-h} values would be predicted to be even lower than 0.1 μM for a system in which only the toroidal hexamer is populated.

Our proposed assembly model (Figure 5) is also consistent with FCS data collected at higher protein concentrations (Figure 1). The K_{h-24} values describing the assembly of hexamers to supramolecular aggregates were estimated to be 4000 μM^3 in the presence of ATPγS but only 25 μM^3 in the presence of ADP. This difference in extracted binding constants provides clear evidence that large aggregate formation is substantially diminished in the presence of ATPγS. It is possible that closed-ring hexamers and open hexameric spirals exist in a dynamic equilibrium as a function of the prevailing ATP/ADP ratio (Figure 5). Alternatively, it is also possible that the closed hexamer constitutes an end product, whereas only open hexameric spirals can continue to grow along the helical axis, for example, by the sequential addition of dimeric units. Third, our data cannot rule out the possibility of coaxial stacking of closed hexameric rings to generate larger complexes. Either way, FCS experiments cannot be utilized to distinguish between these models for supramolecular aggregate formation.

Several studies on AAA+ proteins have demonstrated that toroidal hexameric assemblies have a tendency to sample asymmetric conformational states.[10,54] Therefore, ring closure may be accommodated by individual chains adopting different structural substates that allow for the optimization of intermolecular contacts.[48] In this way, variations in the type of bound nucleotide may facilitate hinge-bending motions coupled to the reaction cycle, and the thermal accessibility of a large variety of different substates may be necessary for proper function.[48] A corollary of a biologically driven mandate for cyclic conformational change is that incorrectly assembled states may form more readily in the test tube. This effect may be more pronounced in the presence of nonbiological nucleotides or if the nucleotide is restricted to one type only (see below).

To Generate Tightly Bound Hexameric Assemblies, Subunit Contacts Must Be Mediated by Magnesium Ions. Although Mg^{2+} coordination to the ATP β- and γ-phosphoryl groups has long been known to aid in substrate binding and hydrolysis, the role of Mg^{2+} in promoting productive assembly remains poorly understood. For 45 μM cotton β-Rca-AC-D173N at a ratio of 3:1 ATP/ADP, low Mg^{2+} leads to supramolecular complex formation, whereas Mg^{2+} in excess of nucleotide coordination favors smaller oligomers consistent with hexameric forms (Figure 3). Strikingly, the estimated dissociation constant for binding of the second magnesium ion lies between 1 and 3 mM, likely within the range of physiological Mg^{2+} fluctuations in the chloroplast stroma believed to occur in response to light/dark adaptation.[23,56] Therefore, we propose that *in vivo*, Rca activity may be adjusted by magnesium-mediated changes in subunit contacts. To the best of our knowledge, magnesium ions have not previously been implicated in mediating chain−chain interactions in other AAA+ proteins, although Mg^{2+} activation of Rca hydrolytic activity has been noted some years ago.[25]

Although a structural model of ATP-bound Rca remains unavailable, the apo-structure of the tobacco Rca AAA+ domain (PDB ID 3T15 and PDB ID 3ZW6)[30] reveals the presence of numerous highly conserved acidic residues near the active site (Figure 6). Some of these, such as Asp288, could participate in the coordination of a second magnesium ion close to a subunit interface, such as by interaction with neighboring-chain Asp242. Although in ClpA, a second Mg^{2+} binding site has been identified on the surface of the N-domain and within 10 Å of bound ADP,[57] it is not clear whether this site would persist with bound ATP, nor whether the second site has the potential to partake in subunit contacts.

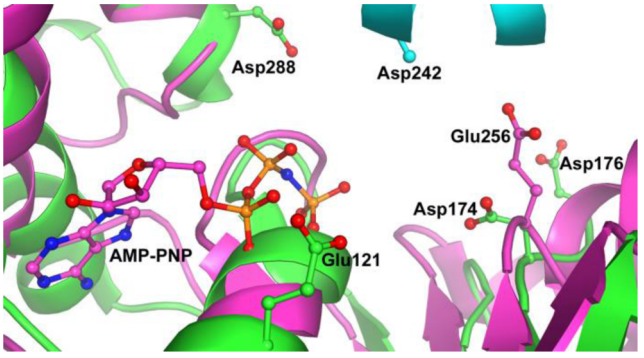

Figure 6. Structural superimpositions of nucleotide-bound FtsH and tobacco Nt-apo-β-Rca. (magenta) Cartoon depicting the structure of the AMP-PNP-bound AAA+ module from FtsH (PDB ID 1IY0). The ATP analog AMP-PNP and the catalytic Glu256 of the Walker B motif are represented in ball-and-stick format. (green) AAA+ module of Nt-apo-β-Rca (PDB ID 3T15) with the catalytic Asp174 of the Walker B motif and additional conserved acidic residues (Glu121, Asp176, and Asp288) represented in ball-and-stick format. (cyan) Adjacent Nt-apo-β-Rca protomer at the crystallographic interface showing the proximity of conserved Asp242 (side chain modeled to Cβ only) to the nucleotide binding pocket. Figure prepared with the PyMOL Molecular Graphics System, Schrödinger, LLC.

AMP-PNP Appears to Promote Non-Native Conformations, Whereas Small Amounts of ADP May Be Critical for Functionally Relevant Ring Asymmetry. We have observed that Alexa-dye derivatization in the presence of AMP-PNP results in double-labeling of β-Rca-AC, indicative of partial protein unfolding. In support of this notion, myosin was reported to undergo active site rearrangements in the presence of this analog.[58] In addition, AMP-PNP appeared to bind only weakly to the cotton β-Rca-AC active site. In the absence of Mg^{2+}, Thermofluor assays suggest that nucleotides interact with

dx.doi.org/10.1021/bi500968h | *Biochemistry* XXXX, XXX, XXX−XXX

Rca with decreasing affinity according to the series ADP > ATPγS > ATP > AMP-PNP (Tables 1 and 2, monitored at 2 mM nucleotide).[24] The addition of Mg^{2+} increases the affinity for ATP, decreases the affinity for ADP, has no effect on ATPγS binding, and further reduces the affinity for AMP-PNP. Therefore, the presence of excess Mg^{2+} modifies the order to the following series Mg·ATP > Mg·ATPγS > Mg·ADP > Mg·AMP-PNP. We propose that either ADP or AMP-PNP as the sole nucleotide causes a restriction of accessible subunit conformations within the Rca oligomer, in analogy to reports on Vps4.[48] This type of mechanism provides a rationale for the preferential formation of non-native states such as spirals, rather than the closed-ring arrangements thought to be biologically relevant. The ordering of binding strength suggests that active site conformational differences exist that modulate interfacial interactions. In combination, the data presented here support the notion that the simultaneous availability of ATP and ADP may be critical for proper assembly and function. As observed for other ATPases, β-Rca-AC is able to catalyze the slow hydrolysis of ATPγS to ADP[47,58] (Supplementary Table S2, Supporting Information), such that a small amount of ADP is produced under all experimental conditions, thereby facilitating biologically relevant ring asymmetry.

Although Microscopic Binding Constants for Rca Assembly May Vary among Different Plant Species, It Is Not Clear Whether These Variations Are Physiologically Relevant. Although species-specific differences in Rca assembly remain poorly understood, it appears likely that significant differences in K_d values exist. For example, SAXS data reported for tobacco apo-β-Rca at 2.4 μM were consistent with hexameric assemblies,[32] whereas cotton β-Rca-AC appears to require concentrations of ∼30 μM to form substantial amounts of hexamers. Below 500 nM, our data indicate that the β-Rca-AC monomer is the primary species in the presence of both ATPγS and ADP. By contrast, Stotz et al.[30] observed hexameric rings in EM images of tobacco Rca-R294V at approximately 500 nM with either Mg·ATP or Mg·ATPγS. Since no EM images were reported for the parent protein, the data suggest that the R294V substitution facilitates hexamerization at very low concentrations. Recently, we have introduced the homologous R293V substitution into the cotton β-Rca-AC construct and found that this mutation causes partial denaturation and renders the protein incapable of nucleotide binding (Wachter, unpublished data). Therefore, it appears that the R294V effect is relatively specific to tobacco Rca.

The Rca subunit concentration in the chloroplast stroma has been estimated to be 7−21 mg/mL (160−480 μM),[22] whereas that of the Rubisco holoenzyme is thought to be on the order of 500 μM. These values allow for a crude estimate of one Rca hexamer per 10 Rubisco holoenzymes under physiological conditions, where only about 3% of all protein entails Rca, while about 40% consists of Rubisco. Strikingly, stromal Rca concentrations are thought to lie significantly above 100 μM, the highest concentration accessible in our FCS experiments. Since hexamer formation is essentially complete at 30 μM (Figure 1), it appears that *in vivo*, Rca is likely always fully assembled. Therefore, Rca assembly in and of itself may not be directly relevant in the regulation of Rubisco activity. Rather, the adjustment of subunit interactions via nucleotide and magnesium ions may play a critical regulatory role.

CONCLUSIONS

The FCS methodology employed in this study allows, for the first time, for a thermodynamic description of protein self-association in highly polydisperse Rca preparations. From these values (Figure 1), fractional concentrations of oligomeric species can be estimated under a variety of solution conditions. We demonstrate that higher ratios of ATP/ADP facilitate the formation of hexameric species and show that free Mg^{2+} plays a role in promoting hexamer formation at the expense of larger complexes. We hope that this information will be useful in the interpretation of functional data and expect that continued application of this technique will allow for a comprehensive analysis of the factors governing Rca assembly, with the ultimate goal of gaining a better understanding of its interaction with Rubisco.

ASSOCIATED CONTENT

Supporting Information

ATPγS hydrolysis of β-Rca-AC and ATP hydrolysis of β-Rca-AC-D173N incubated on ice, ATPase activity of wild-type and β-Rca-AC-D173N at various ATP concentrations in the presence of 5 mM total Mg^{2+}, Absorbance spectra of acid-denatured β-Rca-AC-D173N in 50% acetonitrile, 50% water, 0.1 % TFA, MALDI spectra of Alexa-labeled and unlabeled β-Rca-AC-D173N, and representative FCS decays obtained using 50 nM labeled β-Rca-AC and increasing amounts of unlabeled β-Rca-AC. This material is available free of charge via the Internet at http://pubs.acs.org.

AUTHOR INFORMATION

Corresponding Author

*Rebekka M. Wachter. Tel: 480-965-8188. Fax: 480-965-2747. E-mail: rwachter@asu.edu.

Author Contributions

§A.M.K. and M.C. contributed equally to this work.

Funding

This work was supported by the Division of Chemical Sciences, Geosciences and Biosciences, Office of Basic Energy Sciences of the U.S. Department of Energy through Grant No. DE-FG02-09-ER16123 to R.M.W. and M.L.

Notes

The authors declare no competing financial interest.

ABBREVIATIONS

Rca, Rubisco activase; ATPγS, adenosine 5′-*O*-[γ-thio]-triphosphate; DTT, dithiotheitol; EDTA, ethylenediaminetetraacetic acid; HEPES, 4-(2-hydroxyethyl)-1-piperazineethanesulfonic acid; AMP-PNP, 5′-adenylyl-imidodiphosphate; PNP, purine nucleoside phosphorylase; P_i, phosphate; BSA, bovine serum albumin; EM, electron microscopy; DLS, dynamic light scattering; FCS, fluorescence fluctuation spectroscopy; SAXS, small-angle X-ray scattering; SLS, static light scattering; Rubisco, ribulose-1,5-bisphosphate carboxylase/oxygenase; RuBP, ribulose-1,5-bisphosphate; MESG, 2-amino-6-mercapto-7-methyl purine riboside; PCH, photon-counting histogram

REFERENCES

(1) Spreitzer, R. J., and Salvucci, M. E. (2002) Rubisco: Structure, regulatory interactions, and possibilities for a better enzyme. *Annu. Rev. Plant Biol. 53*, 449−475.

(2) Parry, M. A., Andralojc, P. J., Scales, J. C., Salvucci, M. E., Carmo-Silva, A. E., Alonso, H., and Whitney, S. M. (2013) Rubisco activity

and regulation as targets for crop improvement. *J. Exp. Biol. 64*, 717−730.
(3) Jordan, D. B., and Ogren, W. L. (1981) Species variation in the specificity of ribulose-biphosphate carboxylase-oxygenase. *Nature 291*, 513−515.
(4) Mueller-Cajar, O., Stotz, M., and Bracher, A. (2013) Maintaining photosynthetic CO_2 fixation via protein remodelling: The Rubisco activases. *Photosynth. Res. 119*, 191−201.
(5) Carmo-Silva, A. E., and Salvucci, M. E. (2013) The Regulatory Properties of Rubisco Activase Differ among Species and Affect Photosynthetic Induction during Light Transitions. *Plant Physiol. 161*, 1645−1655.
(6) Snider, J., and Houry, W. A. (2008) AAA+ proteins: Diversity in function, similarity in structure. *Biochem. Soc. Trans. 36*, 72−77.
(7) Ogura, T., and Wilkinson, A. J. (2001) AAA(+) superfamily ATPases: Common structure-diverse function. *Genes Cells 6*, 575−597.
(8) Ogura, T., Whiteheart, S. W., and Wilkinson, A. J. (2004) Conserved arginine residues implicated in ATP hydrolysis, nucleotide sensing, and inter-subunit interactions in AAA and AAA+ ATPases. *J. Struct. Biol. 146*, 106−112.
(9) Hartman, J. J., and Vale, R. D. (1999) Microtubule disassembly by ATP-dependent oligomerization of the AAA enzyme katanin. *Science 286*, 782−785.
(10) Wang, J., Song, J. J., Seong, I. S., Franklin, M. C., Kamtekar, S., Eom, S. H., and Chung, C. H. (2001) Nucleotide-dependent conformational changes in a protease-associated ATPase HslU. *Structure 9*, 1107−1116.
(11) Babst, M., Wendland, B., Estepa, E. J., and Emr, S. D. (1998) The Vps4p AAA ATPase regulates membrane association of a Vps protein complex required for normal endosome function. *EMBO J. 17*, 2982−2993.
(12) Fodje, M. N., Hansson, A., Hansson, M., Olsen, J. G., Gough, S., Willows, R. D., and Al-Karadaghi, S. (2001) Interplay between an AAA module and an integrin I domain may regulate the function of magnesium chelatase. *J. Mol. Biol. 311*, 111−122.
(13) Kress, W., Mutschler, H., and Weber-Ban, E. (2007) Assembly pathway of an AAA+ protein: Tracking ClpA and ClpAP complex formation in real time. *Biochemistry 46*, 6183−6193.
(14) Lenzen, C. U., Steinmann, D., Whiteheart, S. W., and Weis, W. I. (1998) Crystal structure of the hexamerization domain of N-ethylmaleimide-sensitive fusion protein. *Cell 94*, 525−536.
(15) Hanson, P. I., and Whiteheart, S. W. (2005) AAA+ proteins: Have engine, will work. *Nat. Rev. Mol. Cell Biol. 6*, 519−529.
(16) Iyer, L. M., Leipe, D. D., Koonin, E. V., and Aravind, L. (2004) Evolutionary history and higher order classification of AAA+ ATPases. *J. Struct. Biol. 146*, 11−31.
(17) Wang, J., Song, J. J., Franklin, M. C., Kamtekar, S., Im, Y. J., Rho, S. H., Seong, I. S., Lee, C. S., Chung, C. H., and Eom, S. H. (2001) Crystal structures of the HslVU peptidase-ATPase complex reveal an ATP-dependent proteolysis mechanism. *Structure 9*, 177−184.
(18) Page, A. N., George, N. P., Marceau, A. H., Cox, M. M., and Keck, J. L. (2011) Structure and biochemical activities of *Escherichia coli* MgsA. *J. Biol. Chem. 286*, 12075−12085.
(19) Simonetta, K. R., Kazmirski, S. L., Goedken, E. R., Cantor, A. J., Kelch, B. A., McNally, R., Seyedin, S. N., Makino, D. L., O'Donnell, M., and Kuriyan, J. (2009) The Mechanism of ATP-Dependent Primer-Template Recognition by a Clamp Loader Complex. *Cell 137*, 659−671.
(20) Lee, S. Y., De La Torre, A., Yan, D., Kustu, S., Nixon, B. T., and Wemmer, D. E. (2003) Regulation of the transcriptional activator NtrC1: Structural studies of the regulatory and AAA+ ATPase domains. *Genes Dev. 17*, 2552−2563.
(21) Wang, Z. Y., Ramage, R. T., and Portis, A. R. (1993) Mg(2+) and Atp or Adenosine 5′-[Gamma-Thio]-Triphosphate (Atp-Gamma-S) Enhances Intrinsic Fluorescence and Induces Aggregation Which Increases the Activity of Spinach Rubisco Activase. *Biochim. Biophys. Acta 1202*, 47−55.
(22) Portis, A. R. (2003) Rubisco activase - Rubisco's catalytic chaperone. *Photosynth. Res. 75*, 11−27.
(23) Barta, C., Dunkle, A. M., Wachter, R. M., and Salvucci, M. E. (2010) Structural changes associated with the acute thermal instability of Rubisco activase. *Arch. Biochem. Biophys. 499*, 17−25.
(24) Henderson, J. N., Hazra, S., Dunkle, A. M., Salvucci, M. E., and Wachter, R. M. (2013) Biophysical characterization of higher plant Rubisco activase. *Biochim. Biophys. Acta 1834*, 87−97.
(25) Lilley, R. M., and Portis, A. R. (1997) ATP hydrolysis activity and polymerization state of ribulose-1,5-bisphosphate carboxylase oxygenase activase - Do the effects of Mg2+, K+, and activase concentrations indicate a functional similarity to actin? *Plant Physiol. 114*, 605−613.
(26) Li, C., Wang, D., and Portis, A. R. J. (2006) Identification of critical arginine residues in the functioning of Rubisco activase. *Arch. Biochem. Biophys. 450*, 176−182.
(27) Blayney, M. J., Whitney, S. M., and Beck, J. L. (2011) NanoESI mass spectrometry of Rubisco and Rubisco activase structures and their interactions with nucleotides and sugar phosphates. *J. Am. Soc. Mass Spectrom. 22*, 1588−1601.
(28) Mueller-Cajar, O., Stotz, M., Wendler, P., Hartl, F. U., Bracher, A., and Hayer-Hartl, M. (2011) Structure and function of the AAA+ protein CbbX, a red-type Rubisco activase. *Nature 479*, 194−199.
(29) Henderson, J. N., Kuriata, A. M., Fromme, R., Salvucci, M. E., and Wachter, R. M. (2011) Atomic resolution X-ray structure of the substrate recognition domain of higher plant ribulose-bisphosphate carboxylase/oxygenase (Rubisco) activase. *J. Biol. Chem. 286*, 35683−35688.
(30) Stotz, M., Mueller-Cajar, O., Ciniawsky, S., Wendler, P., Hartl, F. U., Bracher, A., and Hayer-Hartl, M. (2011) Structure of green-type Rubisco activase from tobacco. *Nat. Struct. Mol. Biol. 18*, 1366−1370.
(31) Wachter, R. M., Salvucci, M. E., Carmo-Silva, A. E., Barta, C., Genkov, T., and Spreitzer, R. J. (2013) Activation of interspecies-hybrid Rubisco enzymes to assess different models for the Rubisco-Rubisco activase interaction. *Photosynth. Res. 117*, 557−566.
(32) Keown, J. R., Griffin, M. D. W., Mertens, H. D. T., and Pearce, F. G. (2013) Small oligomers of ribulose-bisphosphate carboxylase/oxygenase (Rubisco) activase are required for biological activity. *J. Biol. Chem. 288*, 20607−20615.
(33) Scales, J. C., Parry, M. A. J., and Salvucci, M. E. (2014) A non-radioactive method for measuring Rubisco activase activity in the presence of variable ATP:ADP ratios, including modifications for measuring the activity and activation state of Rubisco. *Photosynth. Res. 119*, 355−365.
(34) Chakraborty, M., Kuriata, A. M., Henderson, J. N., Salvucci, M. E., Wachter, R. M., and Levitus, M. (2012) Protein oligomerization monitored by fluorescence fluctuation spectroscopy: Self-assembly of rubisco activase. *Biophys. J. 103*, 949−958.
(35) Thompson, N. L. (1991) Fluorescence correlation spectroscopy, in *Topics in Fluorescence Spectroscopy* (Lakowicz, J. R., Ed.), Vol. *1*, p 337, Plenum Press, New York.
(36) Muller, J. D., Chen, Y., and Gratton, E. (2003) Fluorescence correlation spectroscopy. *Methods Enzymol. 361*, 69−92.
(37) Gendron, P. O., Avaltroni, F., and Wilkinson, K. J. (2008) Diffusion coefficients of several rhodamine derivatives as determined by pulsed field gradient-nuclear magnetic resonance and fluorescence correlation spectroscopy. *J. Fluoresc. 18*, 1093−1101.
(38) Müller, C. B., Loman, A., Pacheco, V., Koberling, F., Willbold, D., Richtering, W., and Enderlein, J. (2008) Precise measurement of diffusion by multi-color dual-focus fluorescence correlation spectroscopy. *EPL 83*, No. 46001.
(39) Webb, M. R. (1992) A continuous spectrophotometric assay for inorganic phosphate and for measuring phosphate release kinetics in biological systems. *Proc. Natl. Acad. Sci. U.S.A. 89*, 4884−4887.
(40) Salvucci, M. E. (1992) Subunit interactions of Rubisco activase - polyethylene glycol promotes self-association, stimulates ATPase and activation activities, and enhances interactions with Rubisco. *Arch. Biochem. Biophys. 298*, 688−696.
(41) Dawson, R. M. C. (1986) *Data for Biochemical Research*, 3rd ed., Clarendon Press, Oxford.

(42) Salvucci, M. E. (2004) Potential for interactions between the carboxy- and amino-termini of Rubisco activase subunits. *FEBS Lett. 560*, 205−209.
(43) Pulido, N. O., Salcedo, G., Perez-Hernandez, G., Jose-Nunez, C., Velazquez-Campoy, A., and Garcia-Hernandez, E. (2010) Energetic effects of magnesium in the recognition of adenosine nucleotides by the F-1-ATPase beta subunit. *Biochemistry 49*, 5258−5268.
(44) Ericsson, U. B., Hallberg, B. M., DeTitta, G. T., Dekker, N., and Nordlund, P. (2006) Thermofluor-based high-throughput stability optimization of proteins for structural studies. *Anal. Biochem. 357*, 289−298.
(45) Weibezahn, J., Schlieker, C., Bukau, B., and Mogk, A. (2003) Characterization of a trap mutant of the AAA plus chaperone ClpB. *J. Biol. Chem. 278*, 32608−32617.
(46) Dalal, S., Rosser, M. F. N., Cyr, D. M., and Hanson, P. I. (2004) Distinct roles for the AAA ATPases NSF and p97 in the secretory pathway. *Mol. Biol. Cell 15*, 637−648.
(47) Hersch, G. L., Burton, R. E., Bolon, D. N., Baker, T. A., and Sauer, R. T. (2005) Asymmetric interactions of ATP with the AAA+ ClpX6 unfoldase: Allosteric control of a protein machine. *Cell 121*, 1017−1027.
(48) Monroe, N., Han, H., Gonciarz, M. D., Eckert, D. M., Karren, M. A., Whitby, F. G., Sundquist, W. I., and Hill, C. P. (2014) The oligomeric state of the active Vps4 AAA ATPase. *J. Mol. Biol. 426*, 510−525.
(49) Buck, M., and Hoover, T. R. (2010) An ATPase R-Finger leaves its print on transcriptional activation. *Structure 18*, 1391−1392.
(50) Scott, A., Chung, H.-Y., Gonciarz-Swiatek, M., Hill, G. C., Whitby, F. G., Gaspar, J., Holton, J. M., Viswanathan, R., Ghaffarian, S., Hill, C. P., and Sundquist, W. I. (2005) Structural and mechanistic studies of VPS4 proteins. *EMBO J. 24*, 3658−3669.
(51) van de Loo, F. J., and Salvucci, M. E. (1998) Involvement of two aspartate residues of Rubisco activase in coordination of the ATP-g-phosphate and subunit cooperativity. *Biochemistry 37*, 4621−4625.
(52) Goodsell, D. S., and Olson, A. J. (2000) Structural symmetry and protein function. *Annu. Rev. Biophys. Biomol. Struct. 29*, 105−153.
(53) Ali, M. H., and Imperiali, B. (2005) Protein oligomerization: How and why. *Bioorg. Med. Chem. 13*, 5013−5020.
(54) Stinson, B. M., Nager, A. R., Glynn, S. E., Schmitz, K. R., Baker, T. A., and Sauer, R. T. (2013) Nucleotide binding and conformational switching in the hexameric ring of a AAA+ machine. *Cell 153*, 628−639.
(55) Vieux, E. F., Wohlever, M. L., Chen, J. Z., Sauer, R. T., and Baker, T. A. (2013) Distinct quaternary structures of the AAA+ Lon protease control substrate degradation. *Proc. Natl. Acad. Sci. U.S.A. 110*, E2002−E2008.
(56) Ishijima, S., Uchibori, A., Takagi, H., Maki, R., and Ohnishi, M. (2003) Light-induced increase in free Mg2+ concentration in spinach chloroplasts: Measurement of free Mg2+ by using a fluorescent probe and necessity of stromal alkalinization. *Arch. Biochem. Biophys. 412*, 126−132.
(57) Xia, D., Esser, L., Singh, S. K., Guo, F., and Maurizi, M. R. (2004) Crystallographic investigation of peptide binding sites in the N-domain of the ClpA chaperone. *J. Struct. Biol. 146*, 166−179.
(58) Gulick, A. M., Bauer, C. B., Thoden, J. B., and Rayment, I. (1997) X-ray structures of the MgADP, MgATP gamma S, and MgAMPPNP complexes of the Dichyostelium discoideum myosin motor domain. *Biochemistry 36*, 11619−11628.
(59) Keown, J. R., and Pearce, F. G. (2014) Structural characterization of spinach ribulose-1,5-bisphosphate carboxylase/oxygenase activase isoforms reveals hexameric assemblies with increased thermal stability. *Biochem. J.*, DOI: 10.1042/BJ20140676.

■ NOTE ADDED IN PROOF

While this manuscript was under review, a highly relevant study on Rca assembly was published.[59] In the presence of ATPγS, the authors observe hexameric forms of spinach α-Rca and tobacco Rca-R294V at 0.6 μM subunit concentration.